Clim Dyn (2016) 46:83–97
DOI 10.1007/s00382-015-2570-9

Northern East Asian low and its impact on the interannual variation of East Asian summer rainfall

Zhongda Lin[1] · **Bin Wang**[2,3]

Received: 11 December 2014 / Accepted: 16 March 2015 / Published online: 1 April 2015

Abstract The strength of the East Asian summer monsoon and associated rainfall has been linked to the western North Pacific subtropical high (WNPSH) and the lower-tropospheric low pressure system over continental East Asia (EA). In contrast to the large number of studies devoted to the WNPSH, little is known about the variability of the East Asian continental low. The present study delineates the East Asian continental low using 850-hPa geopotential height. Since the low is centered over northern EA (NEA), we refer to it as the NEA low (NEAL). We show that the intensity of the NEAL has large interannual variation, with a dominant period of 2–4 years. An enhanced NEAL exhibits a barotropic structure throughout the whole troposphere, which accelerates the summer-mean upper-tropospheric westerly jet and lower-tropospheric monsoon westerly to its south. We carefully identify the anomalous NEAL-induced rainfall anomalies by removal of the tropical heating effects. An enhanced NEAL not only increases rainfall locally in northern Northeast China, but also shifts the East Asian subtropical front northward, causing above-normal rainfall extending eastward from the Huai River valley across central-northern Japan and below-normal rainfall in South China. The northward shift of the East Asian subtropical front is attributed to the following processes without change in the WNPSH: an enhanced NEAL increases meridional pressure gradients and the monsoon westerly along the East Asian subtropical front, which in turn induces a cyclonic shear vorticity anomaly to its northern side. The associated Ekman pumping induces moisture flux convergence that shifts the East Asian subtropical front northward. In addition, the frequent occurrence of synoptic cut-off lows is found to be associated with an enhanced NEAL. Wave activity analysis indicates that the interannual intensity change of the NEAL is significantly associated with the extratropical Polar Eurasian teleconnection, in addition to the forcing of the tropical WNP heating.

Keywords Northern East Asian low · Western North Pacific subtropical high · East Asian summer monsoon · Subtropical front · Cut-off lows · Polar Eurasian teleconnection

✉ Zhongda Lin
zdlin@mail.iap.ac.cn

[1] State Key Laboratory of Numerical Modeling for Atmospheric Sciences and Geophysical Fluid Dynamics (LASG), Institute of Atmospheric Physics, Chinese Academy of Sciences, Beijing 100029, China

[2] International Pacific Research Center, and Department of Meteorology, University of Hawai'i at Mānoa, Honolulu, HI, USA

[3] Earth System Modelling Center, Nanjing University of Information Science and Technology, Nanjing, China

1 Introduction

East Asia (EA) is located between the Eurasian continent and the North Pacific. This land–sea thermal contrast across EA in summer is represented by the lower-tropospheric low pressure over continental EA and the western North Pacific subtropical high (WNPSH) (Guo 1983). Due to the eastward extension of the continental East Asian low in northern EA (NEA), a south-north gradient of thermal contrast exists over EA between the WNP and NEA (Han and Wang 2007), in addition to the strong east–west thermal contrast (Guo 1983; Shi and Zhu 1996; Zhu et al. 2000; Zhao and Zhou 2005; Cheng et al. 2008). The meridional gradient leads to a strong monsoonal geostrophic westerly and associated heavy rainfall along a subtropical zonal belt over EA

extending eastward from the Yangtze River valley across South Japan (Chen and Huang 2007). Therefore, to better understand the variability of the East Asian summer monsoon and rainfall, it is vital to understand the variability of the land–sea thermal contrast and, consequentially, the low over continental EA and the WNPSH.

Unfortunately, the summer continental East Asian low has rarely been studied, in contrast to much more effort having been devoted to the WNPSH (Lu 2001; Lu and Dong 2001; Wang et al. 2001, 2013a; Yang and Sun 2003; Sui et al. 2007; Zhou et al. 2009; Park et al. 2010; Chung et al. 2011; He et al. 2012; Li et al. 2012; Xiang et al. 2013). Lin (2013) found that during a strong northward jump of the East Asian upper-tropospheric westerly jet in late July, the low pressure is enhanced over NEA, leading to more rainfall in northern Northeast China. In addition, some studies have focused on synoptic cut-off lows over NEA and emphasized their crucial roles in East Asian summer weather and climate (Matsumoto et al. 1982; Bell and Bosart 1989; Price and Vaughan 1992; Sun et al. 1994; Kentarchos and Davies 1998; Chen et al. 2005; Sakamoto and Takahashi 2005; He et al. 2007; Zhao and Sun 2007; Zhang et al. 2008; Hu et al. 2010; Shen et al. 2011). These studies, however, concentrated on synoptic to seasonal variations of the low over continental EA.

Several studies, on the other hand, have already noticed lower-tropospheric circulation changes over continental EA, related to interannual and long-term variability of East Asian summer rainfall (Wu et al. 2010; Shen et al. 2011; Zhu et al. 2011; Wang et al. 2013b; Lin 2014). Shen et al. (2011) showed that the interannual variation of summer rainfall in Northeast China is significantly related to change in the local lower-tropospheric geopotential height. Wu et al. (2010) revealed that increased lower-tropospheric geopotential height over NEA concurs with the decadal rainfall increase in South China after the early 1990s. Recently, Lin (2014) investigated the impacts of summer extratropical disturbances over Eurasia on rainfall in EA. He pointed out that in the positive phases of the Scandinavia, and especially the Polar Eurasian teleconnections, proposed by Barnston and Livezey (1987), lower-tropospheric geopotential height rises up over continental EA and rainfall reduces in northern China. But questions still remain as to whether the rainfall changes in EA are physically linked to the changes of the low over continental EA and, if so, how the low leads to these rainfall responses. In addition, the main features of year-to-year variability of the low over continental EA are also unknown.

The objective of the present study is to understand the year-to-year variability of the low over continental EA. We try to answer the following questions: How do we define the low over continental EA? What are main characteristics of the low's interannual variations and associated spatial structure? What is the impact of the continental East Asian low on East Asian summer rainfall? How does the low affect summer rainfall in EA? The text is arranged as follows. Section 2 introduces the data and methodology used in this study. The characteristics of the interannual variability of the low are investigated in Sect. 3 and the impact of the low on East Asian summer rainfall is explored in Sect. 4. Interpretation of the impact is presented in Sect. 5. Conclusions and further discussion are provided in Sect. 6.

2 Data and methodology

This study uses monthly atmospheric data from the National Centers for Environmental Prediction–National Center for Atmospheric Research (NCEP–NCAR) reanalysis datasets (Kalnay et al. 1996) for the period 1979–2011. In addition, monthly data from the European Centre for Medium-Range Weather Forecasts (ECMWF) 40-year Reanalysis (ERA–40) for 1979–2002 (Uppala et al. 2005) and Interim Reanalysis (ERA-Interim) for 1979–2011 (Dee et al. 2011), as well as the NCEP–Department of Energy (NCEP–DOE) data for 1979–2011 and Japanese 25-year Reanalysis (JRA-25) data for 1979–2004 (Onogi et al. 2007) are also used to verify the results based on the NCEP–NCAR reanalysis data.

Also used are the 6-h specific humidity, zonal and meridional wind at eight pressure levels from 1000 hPa to 300 hPa, and surface pressure data from the NCEP–NCAR reanalysis dataset (Kalnay et al. 1996) for the period 1979–2011. The 6-hourly data are applied to calculate moisture transport and its divergence. Similar to Chen and Huang (2007), the column moisture flux $\boldsymbol{Q}$ is integrated vertically from 300 hPa to the surface,

$$\boldsymbol{Q} = \frac{1}{g}\int_{300}^{Ps} q\boldsymbol{V}dp$$

and its divergence D is calculated as

$$D = \nabla \cdot \boldsymbol{Q} = \frac{1}{g}\nabla \cdot \int_{300}^{Ps} q\boldsymbol{V}dp$$

where q is specific humidity, p is pressure, and $\boldsymbol{V}$ is the horizontal wind vector including zonal (u) and meridional (v) wind components. The constant g is gravitational acceleration and the variable Ps is atmospheric pressure at the surface. The variables $\boldsymbol{Q}$ and D are first calculated at 6-h temporal resolution, and then their seasonal means are derived. When $D > 0$, moisture flux diverges, acting as a sink of moisture; when $D < 0$, it converges, acting as a source of moisture and favors rainfall.

The monthly rainfall data used include the 160-station observed rainfall for mainland China provided by

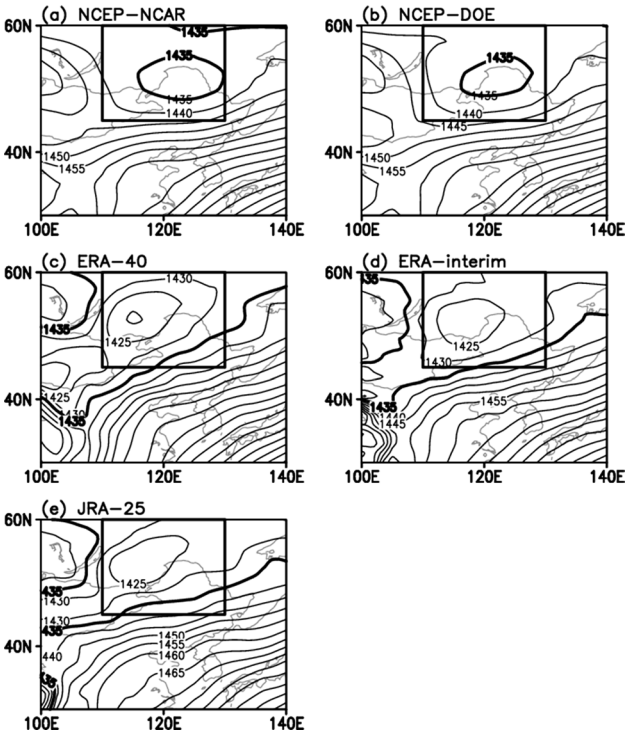

Fig. 1 Climatological summer mean of 850-hPa geopotential height (H850, units: gpm) during 1979–2002 based on **a** NCEP–NCAR, **b** NCEP–DOE, **c** ERA-40, **d** ERA-Interim, and **e** JRA-25 reanalysis data. The *rectangle* depicts the core region of the NEAL

Table 1 Climatological mean and standard deviation (SD) of the intensity of the NEAL, which is defined as the reversed mean 850-hPa geopotential height anomaly (unit: gpm) averaged over the NEAL core region (45°–60°N, 110°–130°E), based on five reanalysis datasets during their shared period of 1979–2002

	NCEP–NCAR	NCEP–DOE	ERA-40	ERA-Interim	JRA-25
Mean	1437	1438	1429	1428	1429
SD	7.98	7.84	9.24	9.01	9.10

the National Climate Center of the China Meteorological Administration and the rainfall derived by the Global Precipitation Climatology Project (GPCP) (Huffman et al. 1997; Adler et al. 2003) during 1979–2011.

In addition, a Polar Eurasian teleconnection index (PEUI) is also used. The Polar Eurasian (PEU) pattern proposed by Barnston and Livezey (1987) is obtained by applying the rotated principal component analysis technique to monthly mean standardized 500-mb height anomalies over the extratropical (20°–90°N) Northern Hemisphere. Its index has been downloaded from the Climate Prediction Center website http://www.cpc.ncep.noaa.gov/data/teledoc/telecontents.shtml.

3 Spatiotemporal characteristics of the interannual variation of the NEA low

3.1 Definition of the NEA low

As shown in Fig. 1a, the low over continental EA is centered over NEA in the summer (June–July–August)-mean 850-hPa geopotential height field based on the NCEP–NCAR reanalysis data. Hereafter we refer to the NEA low as the NEAL. The NEAL is located to the east of the Mongolian highlands, with the central value below 1435 gpm. Similar low centers over NEA are also revealed by the NCEP–DOE (Fig. 1b), ERA-40 (Fig. 1c), ERA-Interim (Fig. 1d), and JRA-25 (Fig. 1e) reanalysis datasets. But the intensity of the NEAL is stronger in the latter three than the former two reanalysis datasets. In addition, the NEAL's centers in the latter three reanalysis datasets are located slightly westward to the east of Lake Baikal, compared with the centers seen over northern Northeast China in the two NECP reanalysis datasets. Here, we define the region (45°–60°N, 110°–130°E) as the core region of the NEAL (Fig. 1). The averaged H850 in the NEAL's core region is 1437 and 1438 gpm based on the NCEP–NCAR and NCEP–DOE reanalysis data respectively, and 1429, 1428, and 1429 gpm based on the ERA-40, ERA-Interim, and JRA-25 reanalysis data (Table 1).

3.2 Interannual variability

The NEAL exhibits strong year-to-year variability (Fig. 2a). The standard deviation of H850 exceeds 10 gpm in the NEAL's core region during 1979–2011 based on the NCEP–NCAR reanalysis data. This strong interannual variability over NEA is also identified in the other four reanalysis datasets (figures not shown). To depict the year-to-year variability of the NEAL's intensity, an index is defined as the reversed mean H850 anomaly averaged over the NEAL core region. The reversed sign is used here so that a positive value of the NEAL index corresponds to a strengthened NEAL. The year-to-year standard deviation of the NEAL index during their common period (1979–2002) is about 8 gpm based on the two NCEP reanalysis datasets and about 9 gpm based on the other three reanalysis datasets (Table 1).

The NEAL's temporal variation is consistent across all five of the reanalysis datasets. All of the correlation coefficients between the NEAL indices calculated from the five reanalysis datasets are greater than 0.9 during their common period of 1979–2002 (Table 2). These correlation coefficients are all significant at the 99.9 % confidence level. Hereafter, the results regarding the interannual variability of the NEAL are presented using the NCEP–NCAR

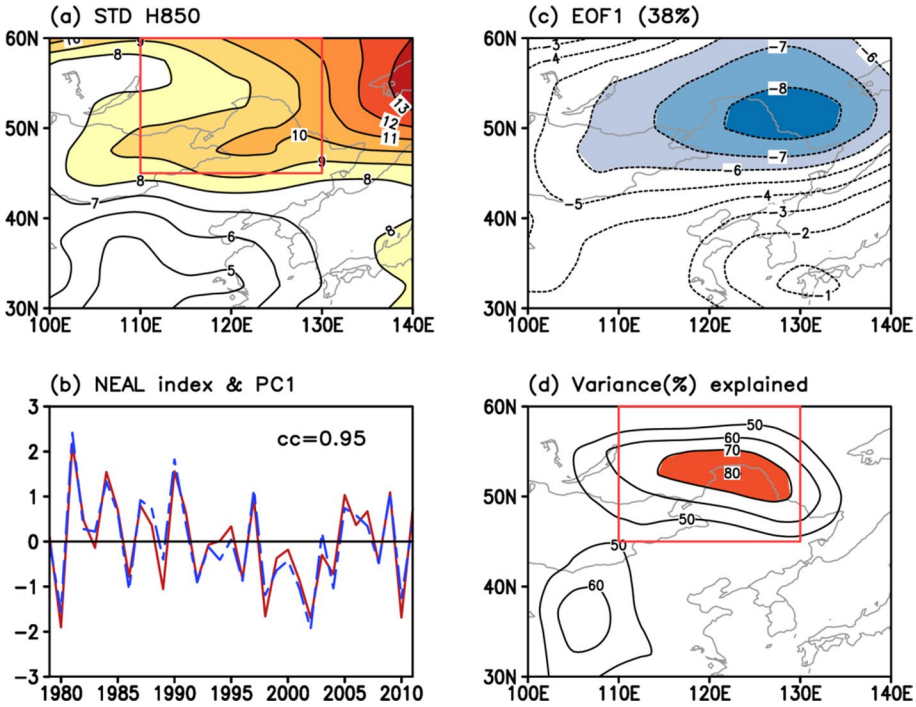

Fig. 2 The standard deviation (**a**), first EOF mode (**c**), and ratio of variance explained by the first EOF mode (**d**) of H850 over subtropical EA and NEA during 1979–2011 based on NCEP-NCAR reanalysis data. **b** Time series of the normalized NEAL index (*blue dashed line*), defined as the reversed mean H850 anomaly averaged over the NEAL core region (45°–60°N, 110°–130°E) as depicted by the *rectangle* in (**a**), and the PC1 corresponding to the first EOF mode (*red solid line*). The correlation coefficient between the NEAL index and the PC1 is 0.95 during 1979–2011

Table 2 Correlation coefficients between the NEAL indices calculated based on the five reanalysis datasets during their shared period of 1979–2002

	NCEP–DOE	ERA-40	ERA-Interim	JRA-25
NCEP–NCAR	0.99	0.95	0.97	0.97
NCEP–DOE		0.93	0.95	0.95
ERA-40			0.98	0.99
ERA-Interim				0.99

reanalysis data only. Similar results are obtained based on the other reanalysis data.

To see whether the NEAL index represents the major mode of variability, we perform an empirical orthogonal functions (EOF) analysis on the H850 anomalies over subtropical EA and NEA (30°–60°N, 100°–140°E). Subtropical EA is divided from NEA by the latitude of 40°N. The first EOF mode is characterized by a negative anomaly over the whole region (Fig. 2b). It explains 38 % of the total variance and is significantly independent of the second EOF mode, which explains 25 % of the total variance (North et al. 1982). Moreover, in the NEAL's core region the first mode explains more than 80 % of its variance (Fig. 2d). The correlation between the principal component corresponding to the first EOF mode (PC1) and the NEAL index during 1979–2011 is 0.95, significant at the 99.9 % confidence level, suggesting that the NEAL index represents the dominant year-to-year variations of H850 over subtropical EA and NEA.

The year-to-year variation of the NEAL index (solid line) is more clearly shown in Fig. 3, which exhibits strong interannual variability. For example, the values of the NEAL index are −11.6 gpm in 1980 and 18 gpm in 1981, which are about −1.5 and 2.5 times its standard deviation of 7.4 gpm during 1979–2011. In addition, the NEAL index also shows a decadal change around the early 1990s. As depicted by the dashed line, its decadal component changes from a positive phase to a negative phase after 1992. Wu et al. (2010) also noticed increased lower-tropospheric geopotential height over NEA, concurrent with a decadal rainfall increase in South China after the early 1990s. This decadal change in the NEAL is partly explained by a warming trend around the Lake Baikal, which is probably due to global warming (Xu et al. 2011a, b; Zhu et al. 2012), and by a shift in the Pacific Decadal Oscillation from a positive phase to a negative phase (Zhu et al. 2011).

In this study, we concern with the interannual variations of the NEAL. The long-term trend and decadal variations with periods longer than 8 years of the seasonal mean anomalies are removed by using Fourier harmonic analysis. Hereafter, the interannual component of the NEAL index is referred to as the NEALI. Figure 4 shows the time-period distribution of the wavelet power spectrum of the NEALI (Fig. 4a) and its global wavelet power spectrum (Fig. 4b). The wavelet basis function used is the sixth-order derivative of a Gaussian function (Torrence and Compo 1998). The wavelet power spectrum is statistically significant at the 95 % confidence level for periods between 2 and 4 years, especially during the 1980s. The global wavelet

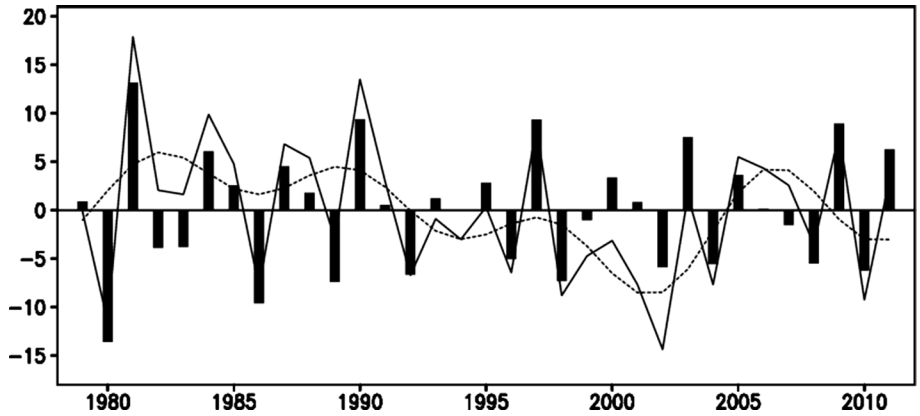

Fig. 3 The unfiltered (*solid line*), interannual component (*bar*), and interdecadal component (*dashed line*) of the NEAL index (unit: gpm). In this study we concentrate on interannual variability and, hereafter, the interannual component of the NEAL index is referred to as the NEALI

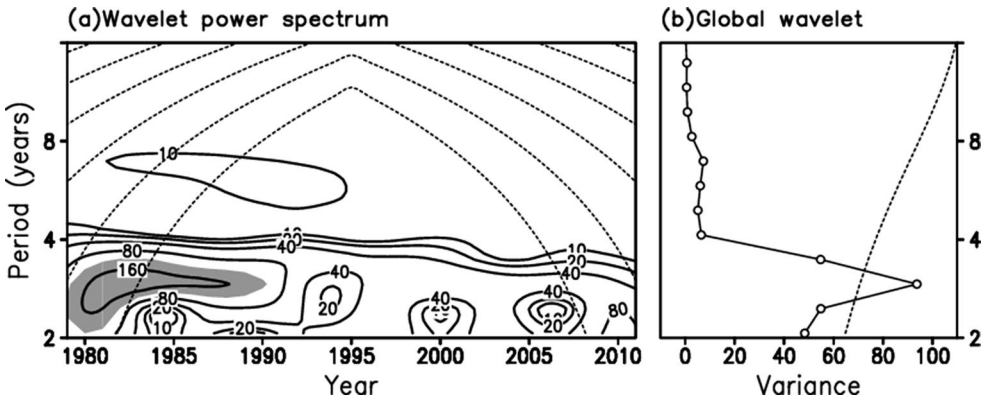

Fig. 4 **a** Wavelet power spectrum of the NEALI. *Dashed lines* indicate the cone of influence outside which edge effects become important and shading depicts significance at the 95 % confidence level. **b** The global wavelet power spectrum of the NEALI (*solid line*). The *dashed line* depicts significance at the 95 % confidence level

power spectrum shows that the NEALI has a dominant energy peak at the period of 2.8 years, suggesting quasi-biennial and quasi-triennial rhythms in the NEAL's intensity change.

3.3 Spatial structure of the NEAL

Figures 5 and 6 present the spatial structure of the anomalous NEAL. Figure 5a shows the H850 anomalies associated with the NEALI. The significant, negative anomaly over NEA indicates intensification of the NEAL. In addition to the change over NEA, the NEALI-related negative H850 anomaly extends westward surrounding the upstream Mongolian highlands and advances southward through subtropical EA to Southeast Asia (Fig. 5a). H850 is also decreased over the subtropical WNP, implying an eastward retreat of the WNPSH (Lu 2001). The correlation between the NEALI and the western extension index of the WNPSH, which is defined as the mean H850 averaged over the domain (10°–30°N, 110°–140°E), the same region of Lu (2001), is −0.39 during 1979–2011, significant at the 95 % confidence level.

Figure 5b further shows the composite H850 difference between positive and negative phases of the NEALI. The 22 years for the composite analysis include 10 positive-phase years when the NEALI is more than 0.5 times its standard deviation, and 12 negative-phase years when the NEALI is less than −0.5 times its standard deviation (Table 3). In the negative phase there is only a weak trough. In the positive phase, H850 in the NEAL's center drops by about 20 gpm compared with that (1445 gpm) in the negative phase. A strong low center appears over NEA, with the minimum being less than 1425 gpm. Therefore, the NEALI realistically represents the interannual variation of the NEAL's intensity. In the positive phase the NEAL is intensified, and vice versa.

Figure 6 shows the three-dimensional structure of the NEALI-related circulation anomalies. There is a significant negative anomaly at 500 hPa (H500) over NEA (Fig. 6a), similar to that at 850 hPa, indicating a barotropic response to an intensified NEAL. The in situ barotropic structure is more clearly identified in the meridionally vertical cross section of the geopotential height anomalies averaged between 110° and 130°E relevant to the NEALI (Fig. 6b). However, the southward-extended negative anomaly over subtropical EA in the lower troposphere reverses in the upper troposphere. The weak, positive geopotential height anomaly appears in the mid and upper troposphere above the pressure level of 600 hPa between 30°N and 40°N. The reversal of the geopotential height anomaly around the mid

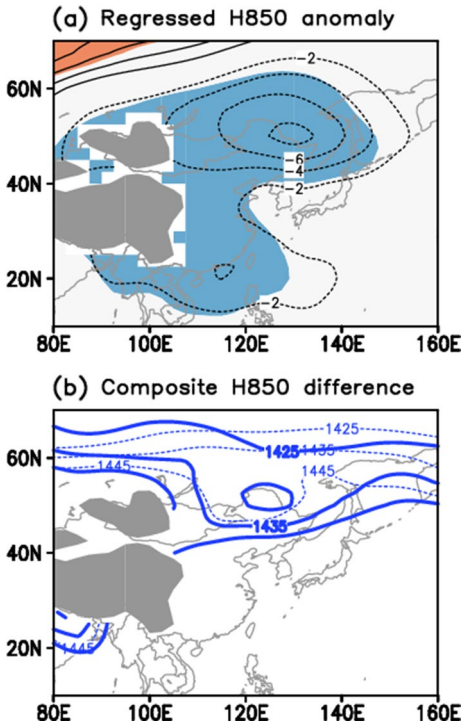

Fig. 5 **a** Regressed H850 anomaly against the normalized NEALI. **b** Composite H850 difference in the positive (*thick solid contours*) and negative (*thin dashed contours*) phases of the NEALI. *Blue* and *orange shadings* in (**a**) denote significant anomalies at the 95 % confidence level and *gray shading* depicts areas with topography exceeding 1500 m

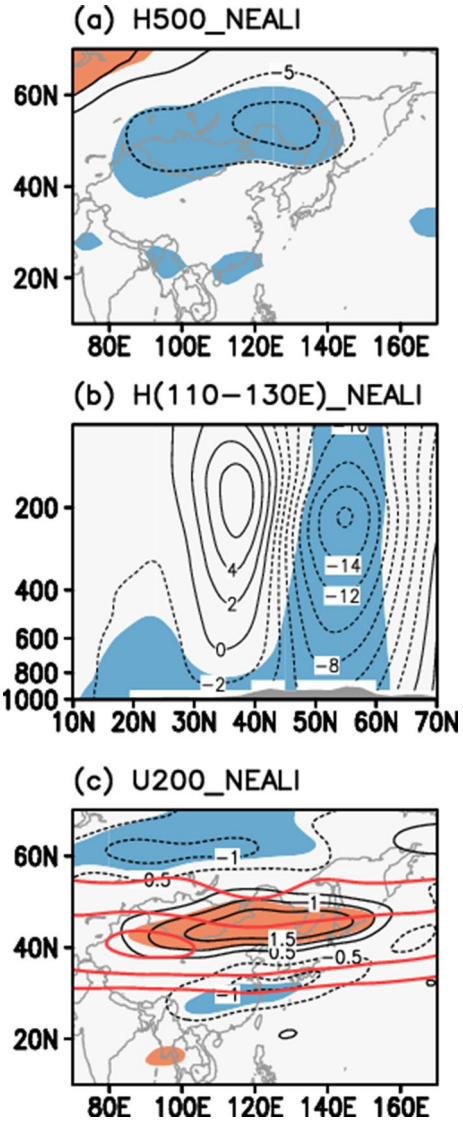

Fig. 6 Same as Fig. 5a, but for regressed anomalies of **a** geopotential height at 500 hPa, **b** zonal-mean meridional profile of the geopotential height averaged between 110°E and 130°E, and **c** zonal wind at 200 hPa against the normalized NEALI. *Red contours* in (**c**) depict the climatological location of the westerly jet at 200 hPa

troposphere is consistent with the NEALI-related insignificant signal of the H500 anomaly over subtropical EA (Fig. 6a). The distribution of the geopotential height anomalies, especially the significant negative anomaly over NEA in the mid–upper troposphere enhances the meridional gradient to the south and, subsequently, the local geostrophic westerly. As expected, a westerly anomaly at 200 hPa over Northeast China is observed (Fig. 6c), which is located within the climatological westerly jet. Thus the upper-tropospheric westerly jet is accelerated over EA.

4 Impact on summer rainfall in East Asia

In the previous section, the results show that the change in the NEAL's intensity decreases the geopotential height in both NEA and subtropical EA, which should affect summer rainfall in EA. In this section, the impact of the NEAL's intensity change on East Asian summer rainfall is investigated. Figure 7a shows the GPCP rainfall anomalies regressed against the NEALI. The intensified NEAL relates to significant positive rainfall anomalies in NEA and negative rainfall anomalies in the Yangtze River valley and the subtropical WNP off the south coast of Japan. These rainfall anomalies in mainland China are confirmed by using 160-station observed rainfall data (Fig. 7b). In addition, rainfall is also enhanced in the tropical WNP, including the South China Sea and the Philippine Sea.

Note that the rainfall anomalies shown in Fig. 7a cannot be totally attributed to the effect of the NEAL because the correlation between the NEALI and the WNP summer rainfall index (WNPSRI), which is defined as the mean rainfall averaged in the tropical WNP region (10°–25°N, 110°–145°E), is 0.61 during 1979–2011, significant at the 99 % confidence level. Many previous works have emphasized

Table 3 Years for the composite analysis (Fig. 5b) based on the NEALI, in which the years in the positive (negative) phase are chosen based on the NEALI being greater (less) than (minus) 0.5 times its standard deviation

Positive phase (10 cases)	Negative phase (12 cases)
1981, *1984*, 1987, *1990*, *1997*, 2000, 2003, *2005*, 2009, *2011*	*1980*, 1982, *1983*, 1986, 1989, 1992, *1996*, *1998*, 2002, 2004, *2008*, *2010*

The *italic* years are related to the WNPSR by the WNPSRI being greater (less) than (minus) 0.5 times its standard deviation in the positive (negative) phase of the NEALI, while the other years underlined, including 4 (6) cases in the positive (negative) phase of the NEALI, are used in the composite analysis in Fig. 9. The WNPSRI is defined as the mean rainfall averaged over the WNP domain (10°–25°N, 110°–145°E)

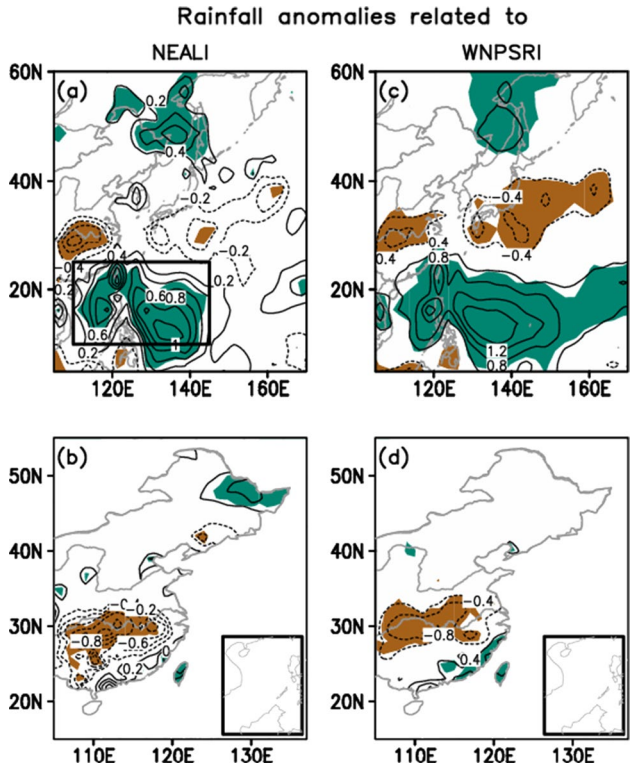

Fig. 7 Rainfall anomalies (units: mm day^{-1}) regressed against **a**, **b** the normalized NEALI and **c**, **d** the normalized tropical WNPSRI. The WNPSRI is defined as the mean rainfall averaged over the domain (10°–25°N, 110°–145°E) depicted by the *rectangle* in (**a**). The *upper panels* (**a**, **c**) are based on GPCP precipitation data and the *bottom panels* (**b**, **d**) are based on 160-station observed precipitation data in mainland China. *Shading* depicts significance at the 95 % confidence level

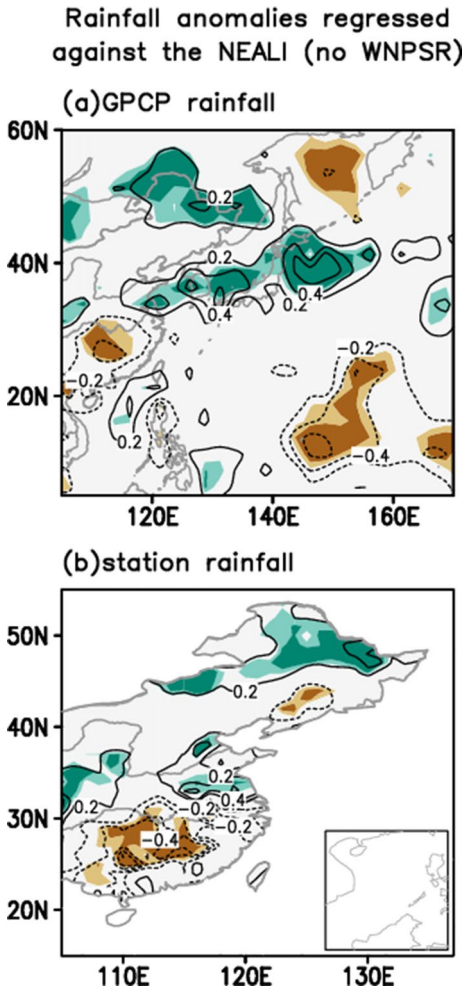

Fig. 8 Same as Fig. 7a, b, but for rainfall anomalies regressed onto the normalized NEALI after removing the effect of the WNPSR. The WNPSR-related component is removed by subtracting linearly regressed anomalies against the WNPSRI. *Light* and *dark shadings* depict significance at the 90 and 95 % confidence levels, respectively

the important influence of tropical WNP heating on East Asian summer rainfall (Nitta 1987; Huang and Sun 1992; Wang et al. 2001; Huang 2004; Ogasawara and Kawamura 2007; Seo et al. 2012). Associated with the WNPSRI, rainfall is reduced zonally along the subtropical East Asian rainy belt from the Yangtze River–Huai River valley across South Japan, and enhanced in the east of NEA (Fig. 7c, d), similar to those related to the NEALI (Fig. 7a, b).

Therefore, it is necessary to exclude the impact of the tropical WNP heating from Fig. 7a. The component related to the WNP summer rainfall (WNPSR) is removed by subtracting the anomalies that linearly regressed onto the WNPSRI. Figure 8a shows the NEALI-related rainfall anomalies after removing the WNPSR impact. For a strong NEAL, the spatial distribution of rainfall anomalies is mainly characterized by a dipole pattern over subtropical EA, with positive rainfall anomalies to the north of the Yangtze River and negative rainfall anomalies in South China. Rainfall is increased significantly along the zonal

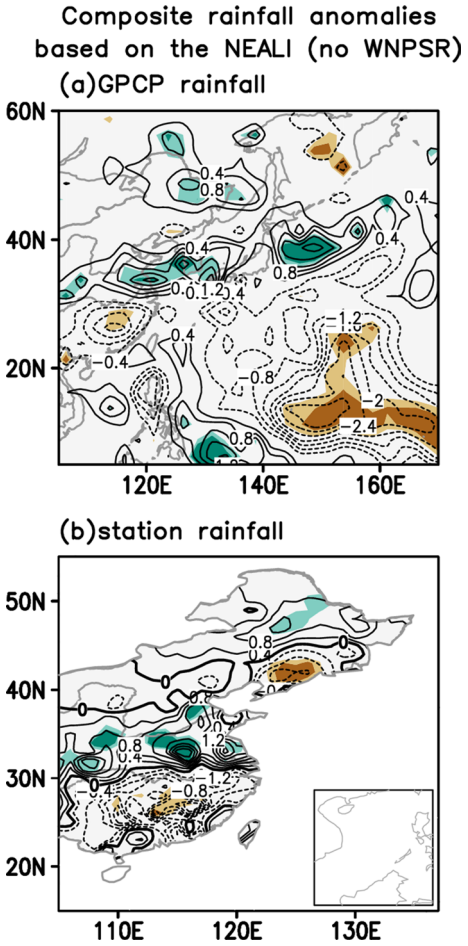

Fig. 9 Composite difference of rainfall between the positive and negative phases of the NEALI without the WNPSR effect based on **a** GPCP precipitation data and **b** 160-station observed rainfall data in mainland China. The cases for the composite are underlined in Table 3, with 4 years in the positive phase and 6 years in the negative phase. *Light* and *dark shadings* represent significance at the 90 and 95 % confidence levels, respectively

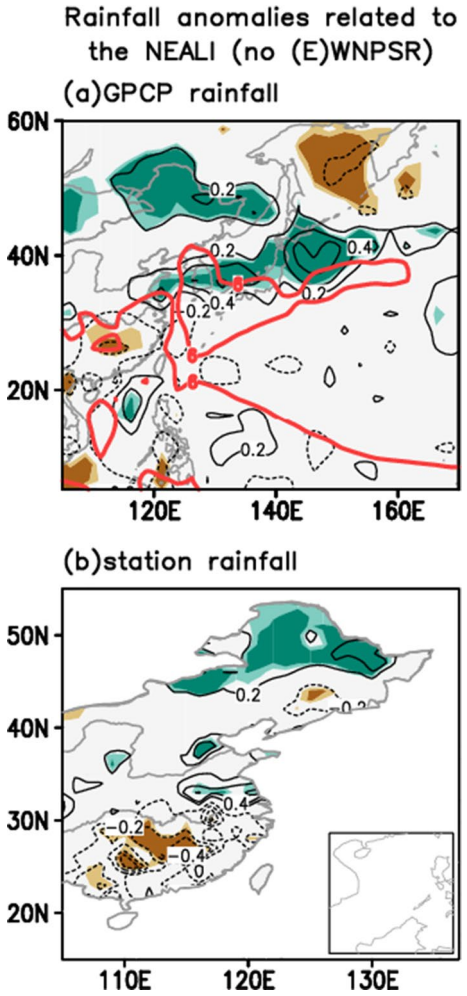

Fig. 10 Same as Fig. 8, but for rainfall anomalies regressed onto the normalized NEALI after removing the effects of both the WNPSR and the EWNPSR. The EWNPSR is represented by the mean rainfall averaged over the EWNP domain (10°–25°N, 145°–160°E). The *bold red contours* in (**a**) depict the location of the climatological East Asian subtropical rainy belt and the intertropical convergence zone over the tropical WNP in summer, in which summer-mean rainfall exceeds 6 mm day^{-1}

belt extending from the Huai River valley across South Korea and Japan until the subtropical WNP off the east coast of Japan. In NEA, rainfall is also increased to the east of Lake Baikal and northern Northeast China. The rainfall responses in mainland China are also supported by those based on 160-station observed rainfall data, with increased rainfall in northern Northeast China and the Huai River valley and reduced rainfall in South China (Fig. 8b).

The independence of the impact of the NEAL from the tropical WNP heating is also illustrated by composite East Asian summer rainfall anomalies based on the NEALI (Fig. 9). The composite is conducted based on four cases without a strong positive WNPSR anomaly in the 10 positive-phase cases of the NEALI, and six cases without a strong negative WNPSR anomaly in the 12 negative-phase cases of the NEALI (Table 3). The increased rainfall to the north of the Yangtze River and in NEA and the decreased rainfall in South China are revealed (Fig. 9), similar to the regressed results after removing the WNPSR impact (Fig. 8).

The composite results also show suppressed rainfall in the tropical eastern WNP (EWNP, east of 145°E) (Fig. 9a), similar to the regressed results in Fig. 8a. To clarify the potential effect of the EWNP summer rainfall (EWNPSR), we regress the rainfall and circulation against the EWNPSR averaged over the domain (10°–25°N, 145°–160°E). There are no significant signals over EA in the related rainfall and circulation anomalies (figures not shown), which suggests the rainfall anomalies shown in Fig. 8a can be primarily attributed to the effect of the

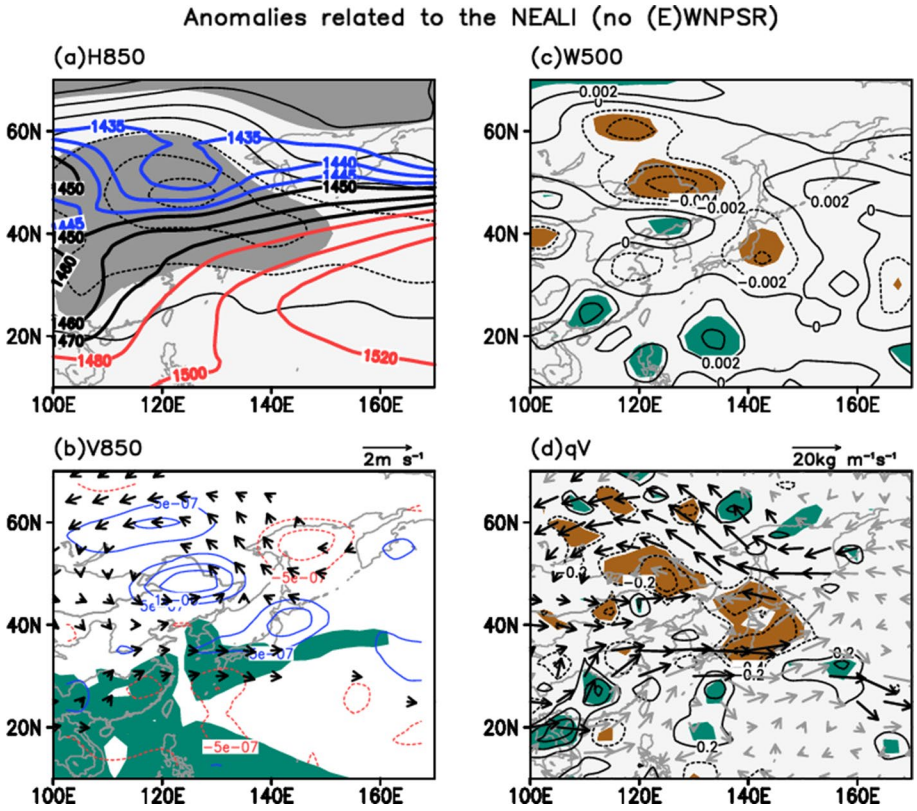

Fig. 11 Same as Fig. 10, but for anomalies of **a** geopotential height and **b** winds (*vector*) and vorticity (*contours*, unit: s^{-1}) at 850 hPa, **c** pressure vertical velocity (units: Pa s^{-1}) at 500 hPa, and **d** column moisture transport integrated vertically from 300 hPa to the surface (*vectors*) and its divergence (*contours*, units: mm day^{-1}). The *thin contour* interval is 2 gpm and the *thick contours* depict the climatology of geopotential height at 850 hPa in summer in (**a**). Wind and moisture transport anomalies with their zonal or meridional components significant at the 95 % confidence level are plotted by *dark vectors* in (**b**) and (**d**), respectively. *Shadings* represent significant anomalies at the 95 % confidence in (**a**, **c**, **d**) and depict the climatological rainy belts with summer-mean rainfall exceeding 6 mm day^{-1} in (**b**)

enhanced NEAL. To confirm this conclusion, we further remove the EWNPSR-related rainfall component, using the same method as that used for removing the WNPSR impact. Figure 10 shows the rainfall anomalies regressed against the NEALI after removing the effects of both the WNPSR and EWNPSR. The spatial pattern of rainfall anomalies is similar to that in Fig. 8, except for the removed EWNP rainfall anomalies. Rainfall increases significantly in NEA related to the enhanced NEAL. In addition, rainfall is also enhanced north of the climatological East Asian subtropical rainy belt in the Huai River valley, South Korea, and especially central-northern Japan. Meanwhile, rainfall is decreased in South China, within and to the south of the climatological subtropical rainy belt. Thus, the East Asian subtropical rainy belt shifts northward related to the intensified NEAL.

Similarly, we also check the NEALI-related monthly rainfall anomalies in June, July, and August after removing the effects of both the WNPSR and EWNPSR (figures not shown). The most significant rainfall signals are seen in July when the peak of rainfall occurs over the East Asian subtropical rainy belt region. The intensified NEAL induces more rainfall to the north of the rainfall belt and less rainfall to the south over South China in July shifting the climatological East Asian subtropical rainy belt northward. In addition, significantly suppressed rainfall over South China is also revealed in August, but not in June. Over NEA, the intensified NEAL leads to increased rainfall in all months from June to August.

5 Interpretation of the result

The question is how does the NEAL result in these rainfall responses? Generally, summer rainfall in continental EA is dominated mainly by the East Asian summer monsoon. The latter is directly tied to two main large-scale circulation systems in the lower troposphere: one is the WNPSH and the other is the NEAL (Fig. 11a). With the subtropical high remaining the same, as the NEAL strengthens, the H850 is not only significantly decreasing in NEA, which results in a cyclonic anomaly with the positive vorticity centered over northern Northeast China (Fig. 11b), but also extending southward to 30°N, confronting the northwest periphery of the WNPSH. This negative H850 anomaly increases the meridional geopotential height gradient between the NEAL and the WNPSH. Accordingly, a geostrophic westerly anomaly is generated along the subtropical East Asian rainy belt at approximately 30°N (Fig. 11b), enhancing the East Asian summer monsoon flow. As a result, a strong cyclonic shear forms to the north, generating a positive vorticity anomaly to the north of the subtropical East Asian rainy belt especially over central-northern Japan. Due to Ekman pumping, lower-tropospheric airflow converges

toward the positive vorticity centers over central-northern Japan and northern Northeast China, forcing ascent over these regions (Fig. 11c). On the other hand, the enhanced monsoon airflow transports more moisture to Japan and east of NEA (Fig. 11d), originated mainly from the Bay of Bengal (figure not shown). Under the favorable conditions of ascending motion and sufficient moisture, column-integrated moisture flux converges over central-northern Japan and northern Northeast China (Fig. 11d), consistent with the increased rainfall in these regions (Fig. 10) and the northward shift of the subtropical East Asian rainy belt. Accompanying the northward shift of the subtropical rainy belt, rainfall decreases to its south, i.e., over South China.

An important persistent synoptic circulation system that affects summer rainfall in NEA is the cut-off low (Matsumoto et al. 1982; Price and Vaughan 1992; Zheng et al. 1992; Sun et al. 1994; Sun and An 2001; Chen et al. 2005; He et al. 2007; Zhao and Sun 2007; Hu et al. 2010, 2011; Shen et al. 2011). Based on the definition of Zheng et al. (1992), a cut-off low event includes: (1) a closed low geopotential height located in the region (30°–65°N, 100°–150°E) at the 500 hPa isobaric surface; (2) a cold core or an evident cold trough accompanying the above-mentioned low. Hu et al. (2010) showed that, climatologically, cut-off lows account for more than 20 % of the summer rainfall in Northeast China. Figure 12a shows the NEALI-related days of cut-off lows in NEA after removing the effects of both the WNPSR and EWNPSR. Associated with the intensified NEAL, cut-off lows occur more frequently in northern NEA and less frequently in the south. The increase in days of cut-off lows favors rainfall over northern Northeast China, in good agreement with the enhanced rainfall related to the strengthened NEAL (Fig. 10). Similarly, the decrease in days of cut-off lows suppresses rainfall over southern Northeast China (Fig. 10b). The response of cut-off lows can possibly be attributed to the enhanced NEAL-induced westerly anomaly at 40°N, which accelerates the climatological East Asian westerly jet (Fig. 12b). The cyclonic meridional shear to the north of the westerly anomaly then favors the occurrence of cut-off lows while the anticyclonic shear to the south suppresses their occurrence.

In summary, the intensity change of the NEAL, independent from the WNP forcing, induces significant rainfall responses in the East Asian region on the interannual timescales. The independence of the variation of the NEAL is related to a wave train over the mid–high latitudes of the Eurasian continent (Fig. 13a). To reveal the characteristics of the associated Rossby wave propagation, the zonal and meridional components of a wave-activity flux for stationary Rossby waves ($\boldsymbol{W}$) are employed following Takaya and Nakamura (2001), which is defined as

$$\boldsymbol{W} = \frac{1}{2|\overline{\boldsymbol{V}}|}\begin{pmatrix} \overline{u}(\psi_x'^2 - \psi'\psi_{xx}') + \overline{v}(\psi_x'\psi_y' - \psi'\psi_{xy}') \\ \overline{u}(\psi_x'\psi_y' - \psi'\psi_{xy}') + \overline{v}(\psi_y'^2 - \psi'\psi_{yy}') \end{pmatrix},$$

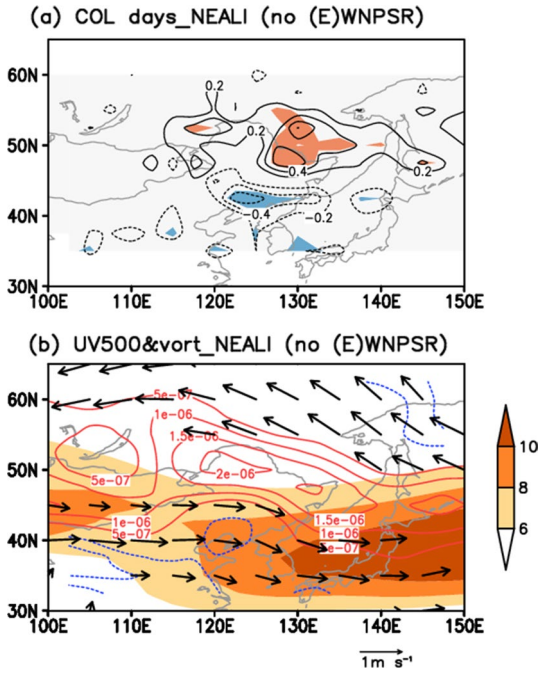

Fig. 12 Same as Fig. 10, but for anomalies of **a** cut-off low (COL) days and **b** winds (*vectors*) and vorticity (*contours*, unit: s^{-1}) at 500 hPa superimposed on the climatology of zonal wind at 500 hPa (*shading*, units: m s^{-1}). *Shadings* represent significance at the 95 % confidence in (**a**), while only wind anomalies with their zonal or meridional components significant at the 95 % confidence level are plotted in (**b**)

where $|\boldsymbol{V}|$ is the magnitude of the horizontal vector wind (u, v) and ψ is the stream function; variables with an overbar represent their climatological summer mean averaged during 1979–2011; variables with subscript and prime notations signify their partial derivatives and anomalies associated with the NEALI after removing the effects of both the WNPSR and EWNPSR, respectively. As shown in Fig. 13b, the wave activity flux emanates from Southern Europe and propagates northeastward through Eastern Europe and Siberia, and then diverts southeastward before finally reaching NEA. Associated with the Rossby wave propagation, four centers are formed with two positive geopotential height anomalies over Southern Europe and western Siberia, and two negative geopotential height anomalies over Eastern Europe and NEA, similar to the negative phase of the PEU teleconnection (Fig. 13c) proposed by Barnston and Livezey (1987). The correlation between the NEALI and the PEUI is −0.63 after removing the effects of both the WNPSR and EWNPSR (Fig. 13d), which is significant at the 99 % confidence level. In other words, the interannual intensity change of the NEAL is significantly related to the extratropical PEU teleconnection, in addition to the forcing of the tropical WNP heating.

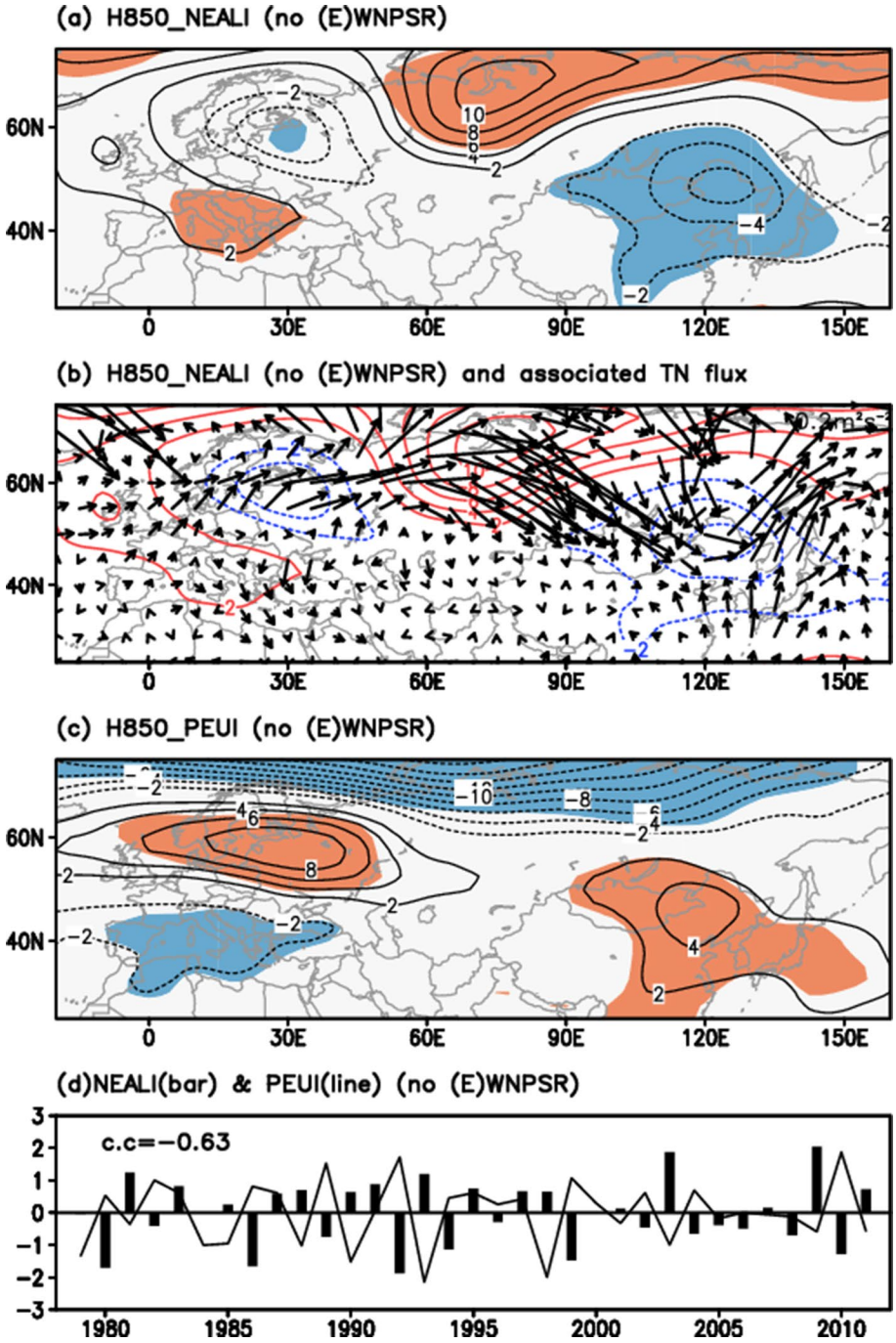

Fig. 13 Same as Fig. 11a, but for **a** H850 anomalies and **b** associated horizontal Takaya and Nakamura (TN) wave flux (*vectors*, Takaya and Nakamura 2001) over the Eurasian continent related to the NEALI. **c** Same as (**a**) but for H850 anomalies related to the PEU teleconnection proposed by Barnston and Livezey (1987). *Shadings* in (**a**, **c**) depict significance at the 95 % confidence levels. **d** Time series of the NEALI (*bars*) and the PEUI (*line*) after removing the effects of both the WNPSR and EWNPSR, with a correlation coefficient of −0.63 during 1979–2011

We further examine the periodicity of the two NEALI components those are related to, and independent of, the WNP heating (Fig. 14), respectively. Similar to the total NEALI in Fig. 4, a significant 2–4-year period is identified in both NEALI components. However, the significant quasi-biennial and quasi-triennial oscillations occurring during the periods of the early 1980s and late 1990s are related to the tropical WNP heating (Fig. 14a), whereas those occurring between the early 1980s and late 1990s (Fig. 14b) are independent of the WNP heating. As discussed in the previous paragraph, the independent component of the NEALI is associated with the PEU teleconnection. Consistent with this finding, we find the PEUI has significant quasi-biennial and quasi-triennial oscillations during the same period of the late 1980s to the mid 1990s when the independent NEALI component exhibits 2–4-year oscillation (Fig. 14b). The results, therefore, indicate a decadal change in the drivers of the interannual variability of the NEAL's intensity; it is dominated by the forcing of the tropical WNP heating during the periods of the early

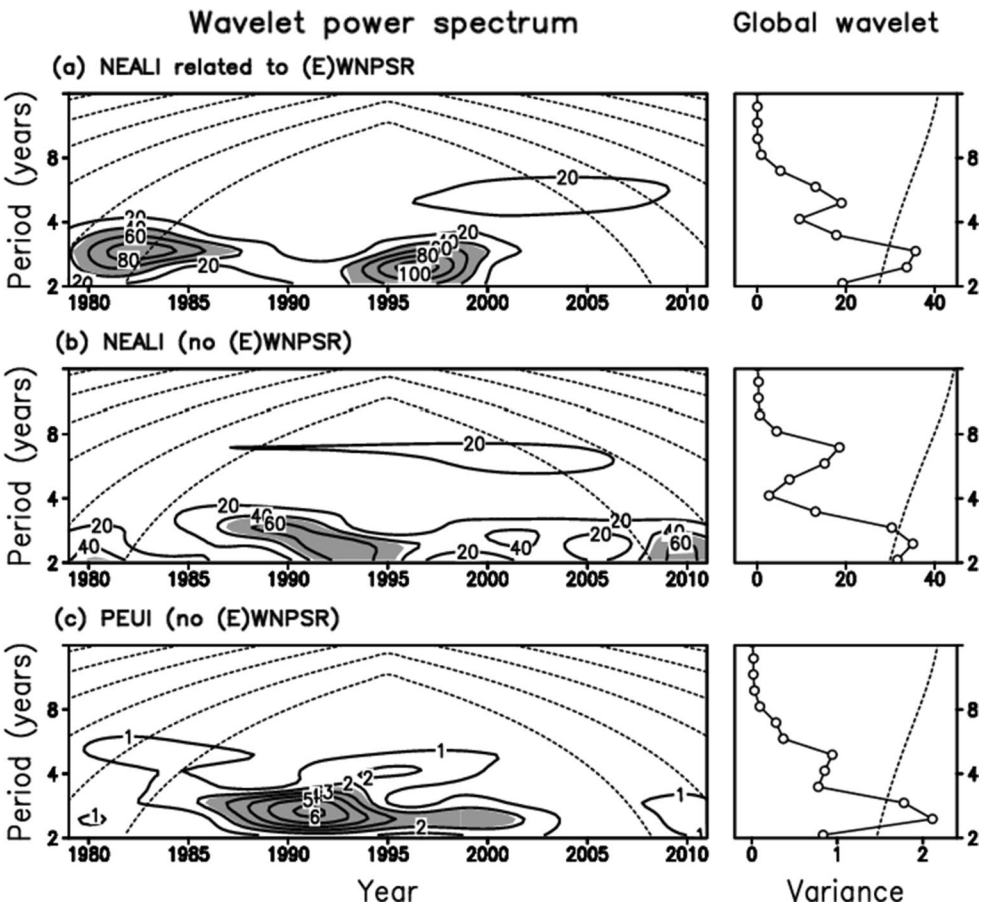

Fig. 14 Same as Fig. 4, but for **a** the NEALI component related to the WNP heating, **b** the NEALI component independent of the WNP heating, and **c** the PEUI after removing the effect of the WNP heating

1980s and late 1990s and by the extratropical circulation during the period of the late 1980s to the mid 1990s.

6 Conclusion and discussion

6.1 Conclusion

This study finds that the summer continental East Asian low, measured by the 850-hPa geopotential height, is centered over NEA. The year-to-year variability of the NEAL is characterized by its intensity change, which approximately explains more than one third of the total variance over subtropical EA and NEA. The wavelet analysis of the NEAL's intensity change shows that its dominant period, on the interannual timescales, is 2–4 years, with the peak at 2.8 years. Associated with the intensified NEAL, geopotential height is decreased significantly in the whole troposphere over NEA, which increases its meridional gradient to the south and then accelerates the East Asian upper-tropospheric westerly jet.

The NEAL's impact on East Asian summer rainfall is also explored. Related to the intensified NEAL, rainfall decreases in NEA, including the southern Russia east of Lake Baikal and northern Northeast China. Meanwhile, the subtropical East Asian rainy belt moves northward. Rainfall is enhanced to the north of the subtropical East Asian rainy belt in the Huai River valley, South Korea, and especially the central-northern Japan, and is reduced within and to the south in South China.

These rainfall responses to the intensified NEAL can be explained by the following physical processes. The intensified NEAL decreases local geopotential height and induces an in situ cyclonic anomaly over NEA in the lower troposphere. On the other hand, the enhanced NEAL also increases its meridional gradient with the WNPSH and, subsequently, the monsoon westerly along the subtropical East Asian rainy belt. The enhanced monsoon westerly induces a cyclonic shear anomaly to the north. Due to lower-tropospheric Ekman pumping and sufficient moisture transported by the enhanced monsoon airflow, moisture flux converges toward the cyclonic anomaly centers over northern Northeast China and to the north of the subtropical East Asian rainy belt. As a result, rainfall increases in NEA and the subtropical East Asian rainy belt moves northward. In South China, the rainfall is deficient probably due to the northward shift of the subtropical East Asian rainy belt. In addition, the intensified NEAL also favors

the more frequent occurrence of synoptic cut-off lows and, subsequently, rainfall over NEA.

The possible mechanism responsible for the interannual variation of the NEAL's intensity is explored. In addition to the effect of the tropical WNP heating, the NEAL's intensity change is also affected by an extratropical Rossby wave train over northern Eurasia, similar to the PEU teleconnection. The NEAL enhances in the positive phase of the PEU pattern and weakens in the negative phase. Moreover, the interannual variation of the NEAL's intensity is significantly associated with the extratropical circulation during the period of the late 1980s to the mid 1990s, while it is modulated by the tropical WNP heating during the periods of the early 1980s and late 1990s.

6.2 Discussion

The present study shows that, corresponding to an intensified NEAL, rainfall decreases along the Yangtze River valley and increases in northern Northeast China (Fig. 7a, b). Considering the interannual variation of the NEAL's intensity is dominated by a component of 2–4-years period (Fig. 4), a triennial oscillation is expected in the associated rainfall in the Yangtze River valley and Northeast China. Some previous studies (Chen et al. 1992; Tian and Yasunari 1992) did find that the interannual variation of rainfall in East China is mostly contributed to by its 2–4-year component. Moreover, Tian and Yasunari (1992) showed that the spatial pattern of the second EOF leading mode (EOF2) of the 2–4-year component of summer rainfall over China is characterized by an out-of-phase change in rainfall over the Yangtze River valley and Northeast China. This EOF2 pattern resembles the NEAL-related rainfall anomalies, suggesting a possible role of the NEAL's intensity change in 2–4-year oscillation of rainfall in these regions. More studies on the relationship between the NEAL and quasi-triennial oscillations in precipitation over China are expected in future studies.

In the present study, we show that the NEAL relates to the tropical WNPSR (Fig. 7). This WNPSR–NEAL relationship is part of the "Pacific–Japan (PJ)" pattern proposed by Nitta (1987) or the "East Asia–Pacific (EAP)" pattern proposed by Huang and Sun (1992). Physically, the tropical heating source that is related to enhanced rainfall over the tropical WNP can excite an extratropical Rossby wave train, with two cyclonic anomalies over the subtropical WNP and NEA, respectively, and an anticyclonic anomaly between them over EA (Huang 2004). The cyclonic anomaly over NEA then intensifies the NEAL, consistent with the positive correlation between the NEALI and the WNPSRI. Associated with this meridional connection, the enhanced NEAL corresponds to deceased rainfall along the subtropical East Asian rainy belt and increased rainfall in the east of NEA (Fig. 7c).

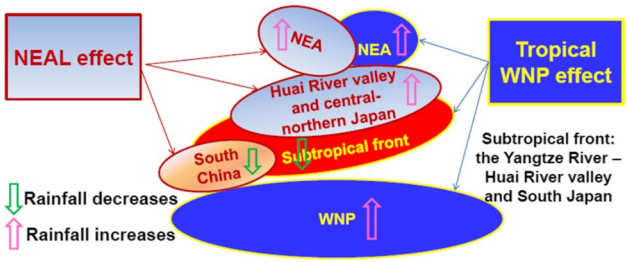

Fig. 15 Schematic diagram showing the effects of an enhanced NEAL and increased rainfall in the tropical WNP

On the other hand, the NEAL can affect summer rainfall in EA independently of the tropical WNP heating. As shown in Fig. 10, after removing the effects of both the WNPSR and EWNPSR, the intensified NEAL leads to an increase of local rainfall and a northward shift of the subtropical East Asian rainy belt. The effect of the NEAL is also independent of that of the WNPSH, since there is no significant change in the WNPSH related to the intensified NEAL (Fig. 11a). Moreover, we identify that the independence of the variation of the NEAL from the tropical WNP forcing can probably be attributed to the extratropical Rossby wave propagation over northern Eurasia. This independence indicates a crucial role of the NEAL individually on the variability of the East Asian summer monsoon and climate.

The interannual variation of the NEAL's intensity, therefore, includes two parts: one related to the tropical WNP forcing, and the other independent of the tropical WNP forcing. Accordingly, rainfall anomalies related to the former can be attributed to the tropical WNP effect, and those associated with the latter to the NEAL effect (Fig. 15). Associated with the enhanced NEAL, the combined effect of the WNP and NEAL results in significantly suppressed rainfall in the Yangtze River valley (the WNP effect) and South China (the NEAL effect) and increased rainfall in NEA (both effects) over continental EA. Over oceanic EA, the significant negative rainfall anomalies induced by the tropical WNP heating (Fig. 7c) offset the positive rainfall anomalies induced by the enhanced NEAL (Fig. 10). As a result, the oceanic EA rainfall anomalies diminish (Fig. 7a).

An investigation is made into the relationship between the interannual variation of the NEAL and the frequency of cut-off lows over NEA. We propose that the enhanced NEAL forms a cyclonic anomaly in the north of NEA, which may provide a favorable seasonal background for frequent occurrence of synoptic cut-off lows. On the other hand, the frequent synoptic cut-off lows decrease the geopotential height over NEA. The climate effect of accumulated decreased geopotential height may strengthen the

summer-mean NEAL. However, this conjecture requires more dynamical diagnosis. In addition, we show that the enhanced NEAL induces significant rainfall anomalies over the subtropical East Asian rainy belt—the region where typical extratropical cyclones, which accompany warm and cold fronts, could also play an important role in producing the enhanced rainfall anomalies. The relationship between the NEAL and typical extratropical cyclones and fronts needs to be clarified and substantiated in future studies.

Acknowledgments The authors appreciate the editor's and two reviewers' comments and suggestions, which led to a much improved manuscript. The authors also thank Dr. Kaixi Hu from the China Meteorological Administration for providing the data on days of cut-off lows in NEA. Z. Lin appreciates the discussion with Prof. Riyu Lu from the Institute of Atmospheric Physics, Chinese Academy of Sciences. This research was supported by the National Natural Science Foundation of China (Grant Nos. 41375086 and 40905025) and the National Basic Research Program of China (Grant No. 2010CB950403). B. Wang acknowledges support from the National Research Foundation (NRF) of Korea through a Global Research Laboratory (GRL) grant of the MEST, #2011-0021927. This is the ESMC publication number 42.

References

Adler RF, Huffman GJ, Chang A, Ferraro R, Xie PP, Janowiak J, Rudolf B, Schneider U, Curtis S, Bolvin D (2003) The version-2 global precipitation climatology project (GPCP) monthly precipitation analysis (1979-present). J Hydrometeorol 4:1147–1167

Barnston A, Livezey R (1987) Classification, seasonality and persistence of low-frequency atmospheric circulation patterns. Mon Weather Rev 115:1083–1126

Bell GD, Bosart LF (1989) A 15-year climatology of northern hemisphere 500 mb closed cyclone and anticyclone centers. Mon Weather Rev 117:2142–2164

Chen JL, Huang R (2007) The comparison of climatological characteristics among Asian and Australian monsoon subsystems. Part II: water vapor transport by summer monsoon. Chin J Atmos Sci 31:766–778

Chen L-X, Dong M, Shao Y-N (1992) The characteristics of interannual variations of the East Asian Monsoon. J Meteorol Soc Jpn 70:397–421

Chen LQ, Chen SJ, Zhou XS, Pan XD (2005) A numerical study ofthe MCS in a cold vortex over northeastern China. Acta Meteorol Sinica 63:173–183

Cheng H, Wu T, Dong W (2008) Thermal contrast between the middle-latitude Asian continent and adjacent ocean and its connection to the East Asian summer precipitation. J Clim 21:4992–5007

Chung P-H, Sui C-H, Li T (2011) Interannual relationships between the tropical sea surface temperature and summertime subtropical anticyclone over the western North Pacific. J Geophys Res 116:D13111. doi:10.1029/2010jd015554

Dee D, Uppala S, Simmons A, Berrisford P, Poli P, Kobayashi S, Andrae U, Balmaseda M, Balsamo G, Bauer P (2011) The ERA-Interim reanalysis: configuration and performance of the data assimilation system. Q J R Meteorol Soc 137:553–597

Guo Q (1983) The summer monsoon intensity index in East Asia and its variation. Acta Geogr Sin 38:207–217

Han J, Wang H (2007) Interdecadal variability of the East Asian summer monsoon in an AGCM. Adv Atmos Sci 24:808–818

He J, Wu Z, Jiang Z, Miao CS, Han GR (2007) "Climate effect" of the northeast cold vortex and its influences on Meiyu. Chin Sci Bull 52:671–679. doi:10.1007/s11434-007-0053-z

He C, Zhou T, Zou L, Zhang L (2012) Two interannual variability modes of the Northwestern Pacific Subtropical Anticyclone in boreal summer. Sci Chin Earth Sci 56:1254–1265. doi:10.1007/s11430-012-4443-y

Hu K, Lu R, Wang D (2010) Seasonal climatology of cut-off lows and associated precipitation patterns over Northeast China. Meteorol Atmos Phys 106:37–48

Hu K, Lu R, Wang D (2011) Cold vortex over Northeast China and its climate effect Chin. J Atmos Sci 35:179–191

Huang G (2004) An index measuring the interannual variation of the East Asian summer monsoon—the EAP index. Adv Atmos Sci 21:41–52

Huang R, Sun F (1992) Impacts of the tropical western Pacific on the East Asian summer monsoon. J Meteorol Soc Jpn 70:243–256

Huffman GJ, Adler RF, Arkin P, Chang A, Ferraro R, Gruber A, Janowiak J, McNab A, Rudolf B, Schneider U (1997) The global precipitation climatology project (GPCP) combined precipitation dataset. Bull Am Meteorol Soc 78:5–20

Kalnay E, Kanamitsu M, Kistler R, Collins W, Deaven D, Gandin L, Iredell M, Saha S, White G, Woollen J (1996) The NCEP/NCAR 40-year reanalysis project. Bull Am Meteorol Soc 77:437–471

Kentarchos AS, Davies TD (1998) A climatology of cut-off lows at 200 hPa in the northern hemisphere, 1990–1994. Int J Climatol 18:379–390

Li W, Li L, Ting M, Liu Y (2012) Intensification of Northern Hemisphere subtropical highs in a warming climate. Nat Geosci 5:830–834. doi:10.1038/ngeo1590

Lin Z (2013) Impact of the two types of northward jumps of East Asian upper-tropospheric jet steam in mid summer on eastern China rainfall. Adv Atmos Sci 30:1224–1234. doi:10.1007/s00376-012-2105-9

Lin Z (2014) Intercomparison of impacts of four summer teleconnections over Eurasia on East Asian rainfall. Adv Atmos Sci 31:1366–1376. doi:10.1007/s00376-014-3171-y

Lu R (2001) Interannual variability of the summertime North Pacific subtropical high and its relation to atmospheric convection over the warm pool. J Meteorol Soc Jpn 79:771–783

Lu R, Dong B (2001) Westward extension of North Pacific subtropical high in summer. J Meteorol Soc Jpn 79:1229–1241

Matsumoto S, Ninomiya K, Hasegawa R, Miki Y (1982) The structure and the role of a subsynoptic-scale cold vortex on the heavy precipitation. J Meteorol Soc Jpn 60:339–354

Nitta T (1987) Convective activities in the tropical western Pacific and their impact on the Northern Hemisphere summer circulation. J Meteorol Soc Jpn 65:373–390

North GR, Bell TL, Cahalan RF, Moeng FJ (1982) Sampling errors in the estimation of empirical orthogonal functions. Mon Weather Rev 110:699–706

Ogasawara T, Kawamura R (2007) Combined effects of teleconnection patterns on anomalous summer weather in Japan. J Meteorol Soc Jpn 85:11–24

Onogi K, Tsutsui J, Koide H, Sakamoto M, Kobayashi S, Hatsushika H, Matsumoto T, Yamazaki N, Kamahori H, Takahashi K (2007) The JRA-25 reanalysis. J Meteorol Soc Jpn 85:369–432

Park J-Y, Jhun J-G, Yim S-Y, Kim W-M (2010) Decadal changes in two types of the western North Pacific subtropical high in boreal summer associated with Asian summer monsoon/El Niño-Southern Oscillation connections. J Geophys Res 115:D21129. doi:10.1029/2009jd013642

Price JD, Vaughan G (1992) Statistical studies of cut-off-low systems. Annu Geophys 10:96–102

Sakamoto K, Takahashi M (2005) Cut off and weakening processes of an upper cold low. J Meteorol Soc Jpn 83:817–834

Seo K-H, Son J-H, Lee S-E, Tomita T, Park H-S (2012) Mechanisms of an extraordinary East Asian summer monsoon event in July 2011. Geophys Res Lett 39:L05704. doi:10.1029/2011gl050378

Shen BZ, Lin ZD, Lu RY, Lian Y (2011) Circulation anomalies associated with interannual variation of early-and late-summer precipitation in Northeast China. Sci Chin Earth Sci 54:1095–1104

Shi N, Zhu Q (1996) An abrupt change in the intensity of the East Asian summer monsoon index and its relationship with temperature and precipitation over East China. Int J Climatol 16:757–764

Sui C-H, Chung P-H, Li T (2007) Interannual and interdecadal variability of the summertime western North Pacific subtropical high. Geophys Res Lett 34:L11701. doi:10.1029/2006gl029204

Sun L, An G (2001) A diagnostic study of Northeast cold vortex heavy rainfall over the Songhuajiang–Nenjiang River basin in the summer of 1998. Chin J Atmos Sci 25:342–354

Sun L, Zheng XY, Wang Q (1994) The climatological characteristics of northeast cold vortex in China. Q J Appl Meteorol 5:297–303

Takaya K, Nakamura H (2001) A formulation of a phase-independent wave-activity flux for stationary and migratory quasigeostrophic eddies on a zonally varying basic flow. J Atmos Sci 58:608–627

Tian S-F, Yasunari T (1992) Time and space structure of interannual variations in summer rainfall over China. J Meteorol Soc Jpn 70:585–596

Torrence C, Compo GP (1998) A practical guide to wavelet analysis. Bull Am Meteorol Soc 79:61–78

Uppala SM, Kållberg P, Simmons A, Andrae U, Bechtold V, Fiorino M, Gibson J, Haseler J, Hernandez A, Kelly G (2005) The ERA-40 re-analysis. Q J R Meteorol Soc 131:2961–3012

Wang B, Wu R, Lau KM (2001) Interannual variability of the Asian summer monsoon: contrasts between the Indian and the western North Pacific–East Asian monsoons*. J Clim 14:4073–4090

Wang B, Xiang B, Lee J-Y (2013a) Subtropical High predictability establishes a promising way for monsoon and tropical storm predictions. Proc Natl Acad Sci USA 110:2718–2722. doi:10.1073/pnas.1214626110

Wang Y, Chen W, Zhang J, Nath D (2013b) Relationship between soil temperature in May over Northwest China and the East Asian summer monsoon precipitation. Acta Meteorol Sin 27:716–724. doi:10.1007/s13351-013-0505-0

Wu R, Wen Z, Yang S, Li Y (2010) An interdecadal change in southern China summer rainfall around 1992/93. J Clim 23:2389–2403

Xiang B, Wang B, Yu W, Xu S (2013) How can anomalous western North Pacific Subtropical High intensify in late summer? Geophys Res Lett 40:2349–2354. doi:10.1002/grl.50431

Xu K, He J, Zhu C (2011a) The interdecadal linkage of the summer precipitation in eastern China with the surface air temperature over Lake Baikal in the past 50 years. Acta Geogr Sin 69:570–580

Xu K, Zhu C, He J (2011b) Impact of the surface air temperature warming around Lake Baikal on trend of summer precipitation in North China in the past 50 years. Plateau Meteorol 30:309–317

Yang H, Sun S (2003) Longitudinal displacement of the subtropical high in the western Pacific in summer and its influence. Adv Atmos Sci 20:921–933

Zhang C, Zhang Q, Wang Y, Liang X (2008) Climatology of warm season cold vortices in East Asia: 1979–2005. Meteorol Atmos Phys 100:291–301. doi:10.1007/s00703-008-0310-y

Zhao SX, Sun JH (2007) Study on cut-off low-pressure systems with floods over Northeast Asia. Meteorol Atmos Phys 96:159–180

Zhao P, Zhou ZJ (2005) East Asian subtropical summer monsoon index and its relationships to rainfall. Acta Meteorol Sin 23:18–28

Zheng XY, Zhang TZ, Bai RH (1992) Rainstorm in Northeast China. Meteorological Press, Beijing

Zhou T, Yu R, Zhang J, Drange H et al (2009) Why the western Pacific subtropical high has extended westward since the late 1970s. J Clim 22:2199–2215

Zhu C, He J, Wu G (2000) East Asian monsoon index and its interannual relationship with large-scale thermal dynamic circulation. Acta Meteorol Sin 58:391–402

Zhu Y, Wang H, Zhou W, Ma J (2011) Recent changes in the summer precipitation pattern in East China and the background circulation. Clim Dyn 36:1463–1473

Zhu C, Wang B, Qian W, Zhang B (2012) Recent weakening of northern East Asian summer monsoon: a possible response to global warming. Geophys Res Lett 39:L09701. doi:10.1029/2012gl051155